

Estimation of Temporally Evolving Typhoon Winds and Waves from Synthetic Aperture Radar

David Walker
SRI International, 2100 Commonwealth Boulevard
Ann Arbor MI 48105
phone: (734) 926-4416 fax: (734) 926-4402 email: david.walker@sri.com

Contract Number: N000014-09-C-0530
<http://sri.com/esd/>

LONG-TERM GOALS

The long term goal is to develop a methodology for using synthetic aperture radar (SAR) data to improve characterization of the winds and waves generated by typhoons in the western Pacific Ocean.

OBJECTIVE

The objective is to develop a variational inversion algorithm based on the SWAN model to estimate the near-surface typhoon wind field from SAR data.

APPROACH

Third-generation wave spectrum models such as SWAN can be used to predict wind-generated waves. Combining SWAN and a model relating the SAR-image spectrum to the computed wave spectrum, one can predict the SAR-image spectrum which results from a known wind field. Using variational techniques, this relationship can be inverted to estimate the wind field from SAR data. This approach uses adjoint versions of the SWAN and SAR models to calculate the gradient of the error of the predicted SAR data with respect to the input wind field. This gradient is used to iteratively adjust the wind field to produce a wave field from SWAN that yields a best-fit to the SAR data.

WORK COMPLETED

An algorithm for estimation of temporally evolving winds has been developed. It is based on an existing algorithm for the SWAN wave model and SAR data, developed to estimate the ocean-wave field for a near-shore region for stationary conditions using SAR data (Walker 2006). The algorithm is variational in nature and is based on the SWAN 40.51 ocean-wave-spectrum model (Ris *et al.* 1999, Booij *et al.* 1999) coupled to the nonlinear SAR-spectrum model of Hasselmann and Hasselmann (1991). In its original form, the algorithm was used to estimate the boundary conditions for SWAN that result in a wave-spectrum prediction which best fits the SAR data. An expression for the gradient of the cost function (the error in the estimates of the data) with respect to the input wind field in terms of the forward and adjoint solution was first developed, and then the algorithm was extended to include wind estimation for non-stationary conditions. This required: (1) extension of the SWAN code to efficiently store the entire five-dimensional forward solution; (2) extension of the adjoint SWAN

solver to work for non-stationary conditions, to read in the forward solution time history, and to ingest observation data at arbitrary locations and times; and (3) development of ancillary codes to calculate the gradient from the forward and adjoint SWAN solutions, adjust the wind field, and control the iteration process. These have been completed. In addition, the wind-wave generation modeling in SWAN (Wu 1982) was updated to include high-wind-speed effects on the drag coefficient correlation consistent with the results of Donelan *et al.* (2004). Application of the resulting algorithm to some of the initial SAR data from the ITOP/TCS10 field experiment has also been completed and is shown below.

RESULTS

The algorithm structure has now been finalized, and a graphical description is shown Figure 1. The algorithm makes use of operation forecast data (as a first guess for winds), models and adjoint models (the SWAN wave spectrum model and the Hasselmann & Hasselmann 1991 SAR spectrum model and corresponding adjoints), ancillary data such as bathymetry, and SAR data (presently obtained from CSTARs). The algorithm outputs are wind and wave products: improved wave spectra and improved estimates of the wind field. Estimates begin with a first guess wind field for the region obtained from operational wind forecasts. An estimate of the wave spectrum and the SAR image spectrum are calculated. The SAR spectrum is compared to that for the data (from CSTARs) and the difference is fed back through adjoint SAR and SWAN models. The gradient of the error in the estimated SAR spectrum with respect to the wind field is calculated from the adjoint wave spectrum. This gradient is used to adjust the wind field using a descent algorithm and the steps are repeated until the wind field converges and the SAR spectrum is a best fit.

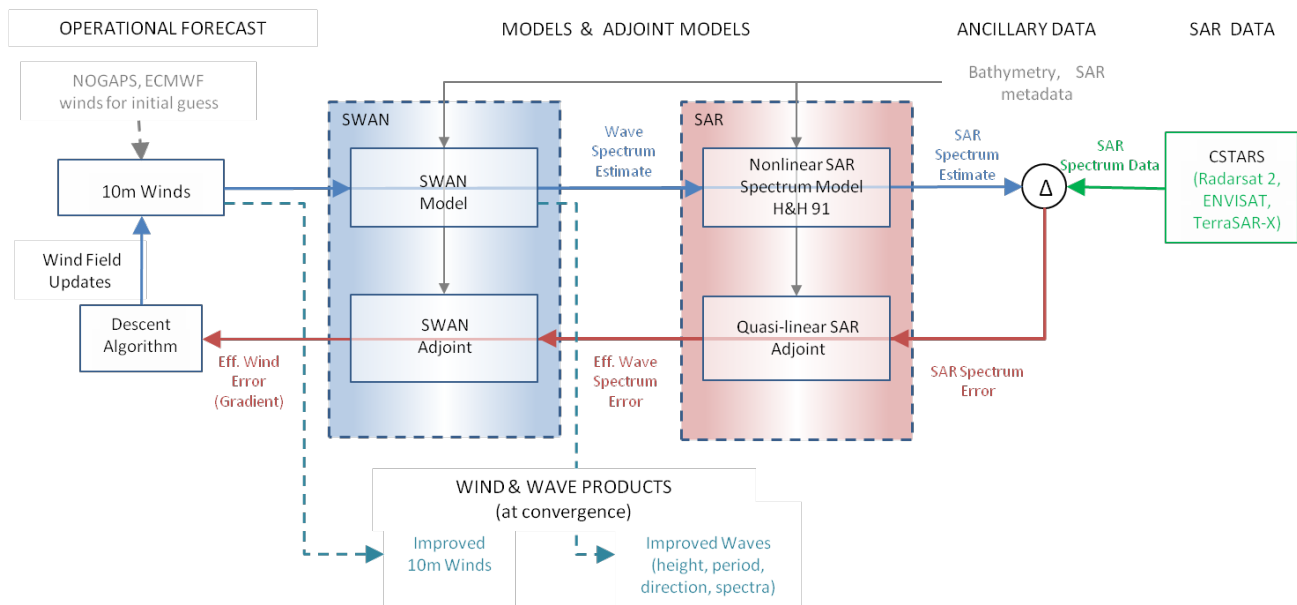


Figure 1. Algorithm flow chart. The algorithm makes use of operation forecast data (as a first guess for winds), models and adjoint models (the SWAN wave spectrum model and the Hasselmann & Hasselmann 1991 SAR spectrum model and corresponding adjoint models), ancillary data (such as bathymetry), and SAR data, (presently obtained from CSTARs). The algorithm outputs are wind and wave products, improved wave spectra and improved estimates of the wind field.

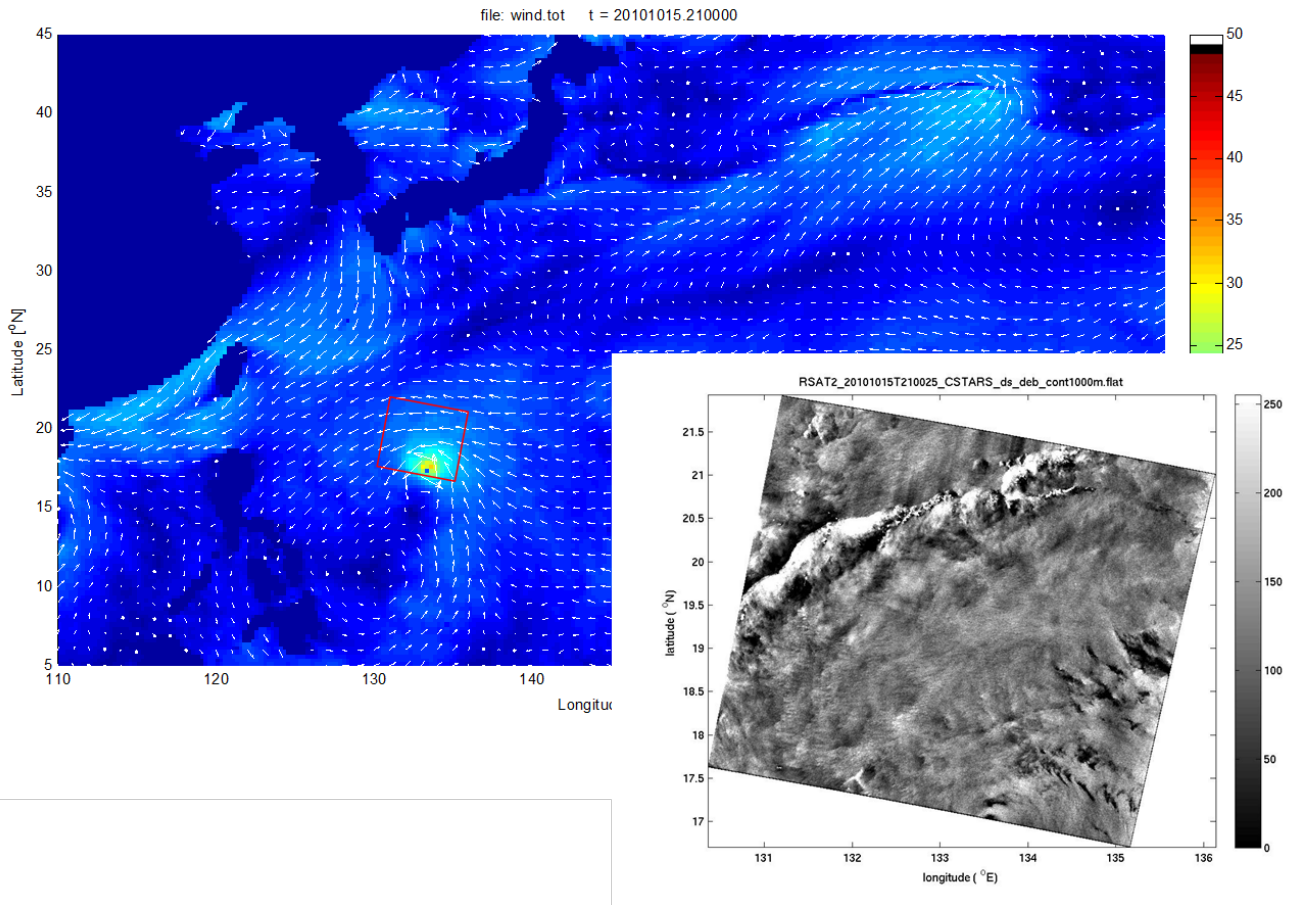


Figure 2. ECMWF winds and a Radarsat-2 SAR image for 2100 GMT during Typhoon Megi on 15 October 2010. The red box on the wind field shows the location of the SAR image, and the ECMWF maximum winds are about 32 m/s.

The algorithm has been applied to Radarsat-2 data for Typhoon Megi at 2100 GMT on 15 October 2010. A second Radarsat-2 data set for Megi at 2142 GMT on 17 October 2010 has also been analyzed but will not be shown in detail here. The SWAN model is run with a one-hour time step on a 0.25 degree grid using bathymetry derived from the GEBCO 30 arcsec database, smoothed and interpolated onto a 0.125 degree grid. The initial guess for the winds is based on ECMWF operational forecast data, consisting of analysis fields at 0000 GMT and 1200 GMT and forecast fields at the intervening three-hour intervals, all on a 0.25 degree grid; linear interpolation is used in SWAN to calculate the winds at one-hour intervals. Figure 2 shows the winds for 2100 GMT on 15 October, along with the Radarsat-2 SAR image, with the location of the SAR image shown on the wind field. As can be seen the eye of the storm is located near the southern boundary of the SAR image, but the image contains most of the high-wind speed region in the right-front quadrant of the storm.

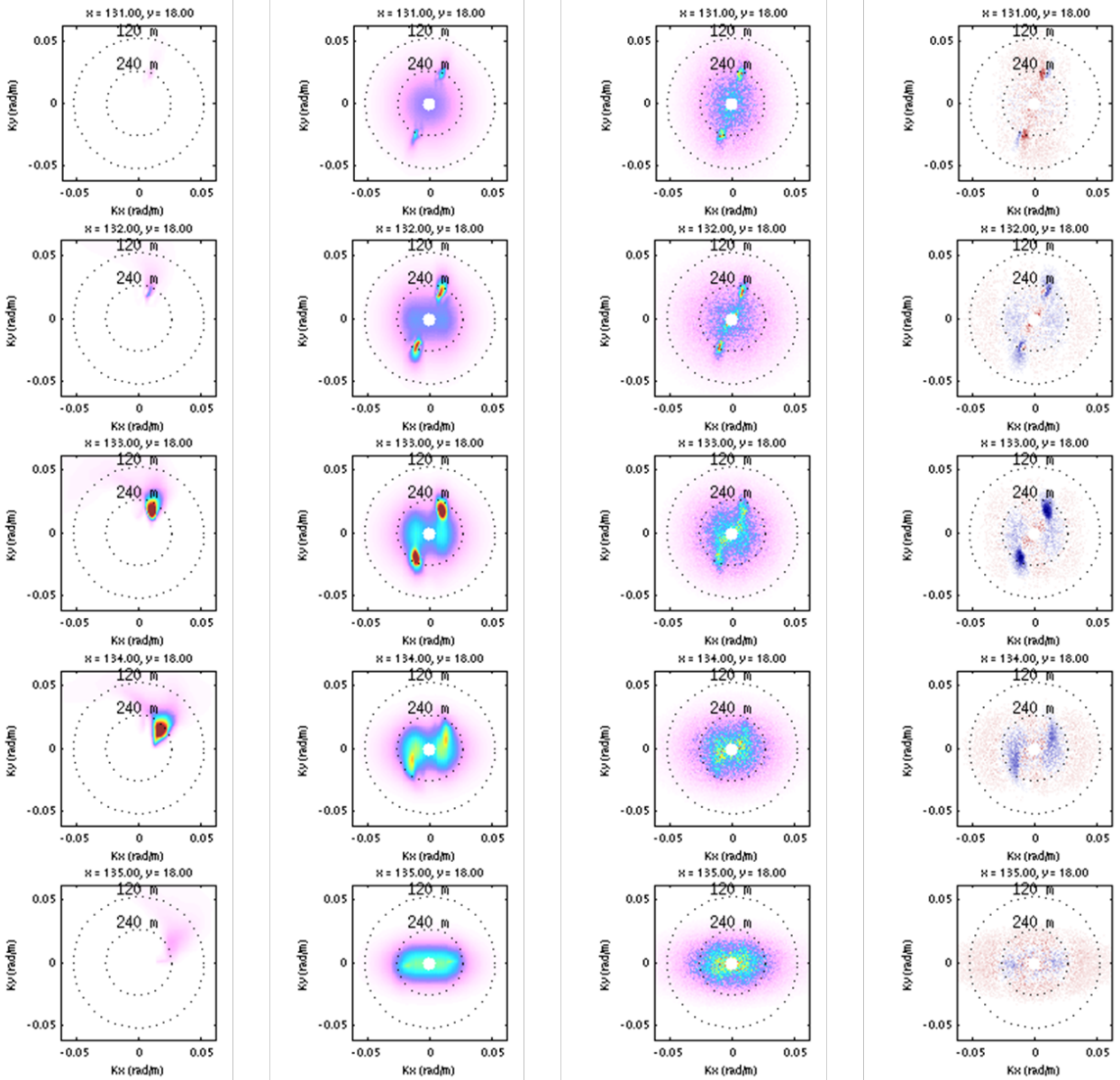


Figure 3. Comparison of estimated and observed SAR spectra for initial-guess ECMWF winds for Typhoon Megi on 15 October 2010 at 18 deg N and various longitudes. From left to right: estimated ocean wave spectra, estimated SAR spectra, observed SAR spectra and difference between estimates and observed SAR spectra.

Figure 3 shows wavenumber spectra for various quantities at integer longitudes and 18 degrees N latitude in the region of the SAR image for the initial-guess winds. (The wavenumber axes are range direction on the ordinate and azimuth direction on the abscissa.) From left to right are shown the wave spectra, the estimated SAR spectra, the observed SAR spectra and the difference between the estimated and observed SAR spectra. A large variation in significant wave height is in evidence as is a large variation in imaging geometries. The SAR model performs well as evidenced in the difference spectra which indicate the largest source of error corresponds to the wave spectrum (not the portion of the spectrum representing speckle noise).

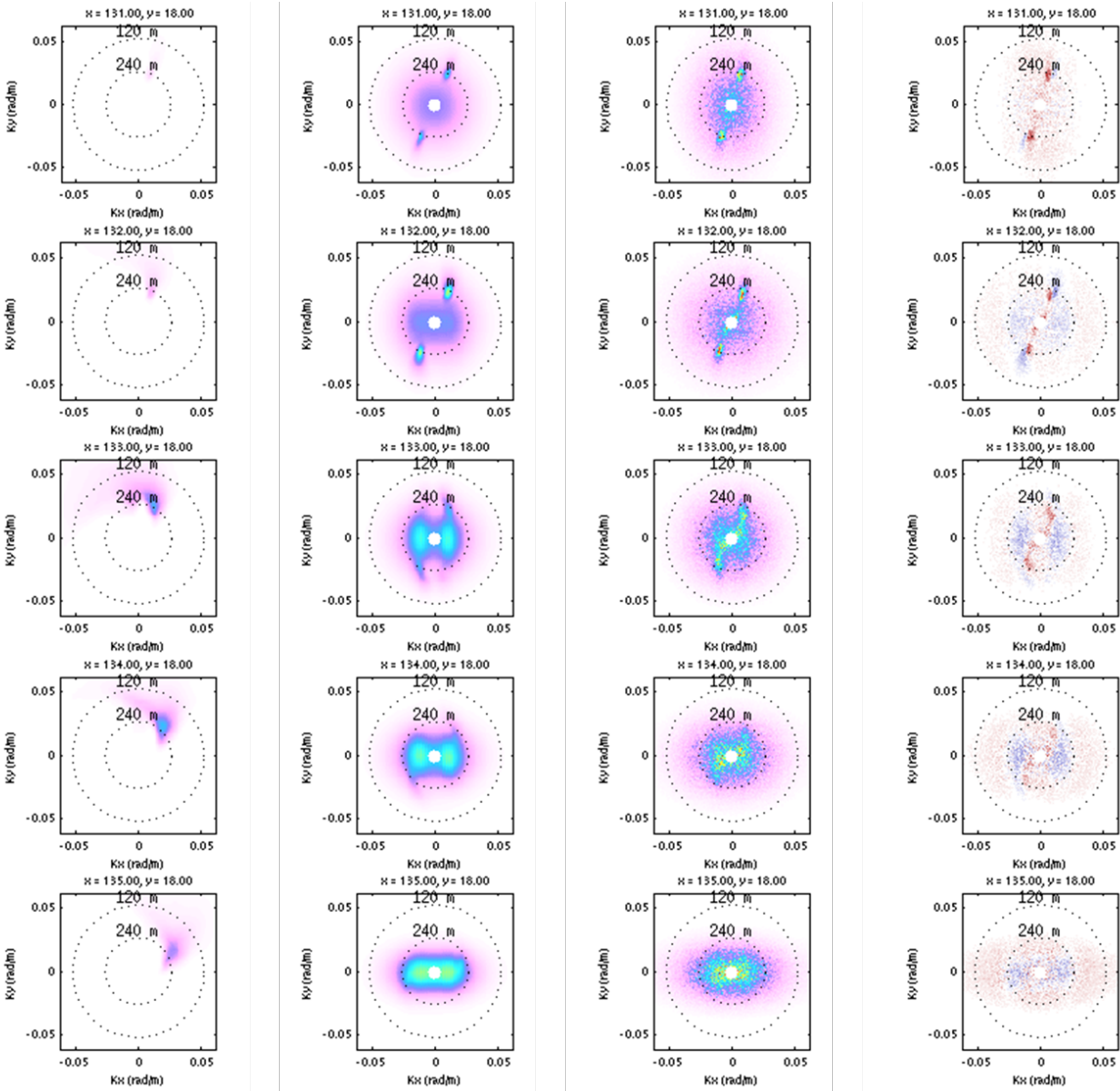


Figure 4. Comparison of estimated SAR spectra using SWAN/SAR winds for Typhoon Megi on 15 October 2010 at 18 deg N and various longitudes. From left to right: estimated ocean wave spectra, estimated SAR spectra, observed SAR spectra and difference between estimates and observed SAR spectra.

A comparison of spectra similar to that shown in Figure 3 is shown for the final estimated winds in Figure 4. Again spectra are shown for integer longitudes at 18 deg N in the area of the SAR image, and from left to right they correspond to estimated wave spectra, estimated SAR-image spectra, observed SAR-image spectra, and the difference between the estimated and observed SAR spectra. Here we can see that the wave spectra have decreased in significant wave height, and the agreement between the predicted and observed SAR spectra has improved. The decrease in wave height can be traced to lower estimated winds at earlier times even though, as will be shown below, the contemporaneous winds have increased.

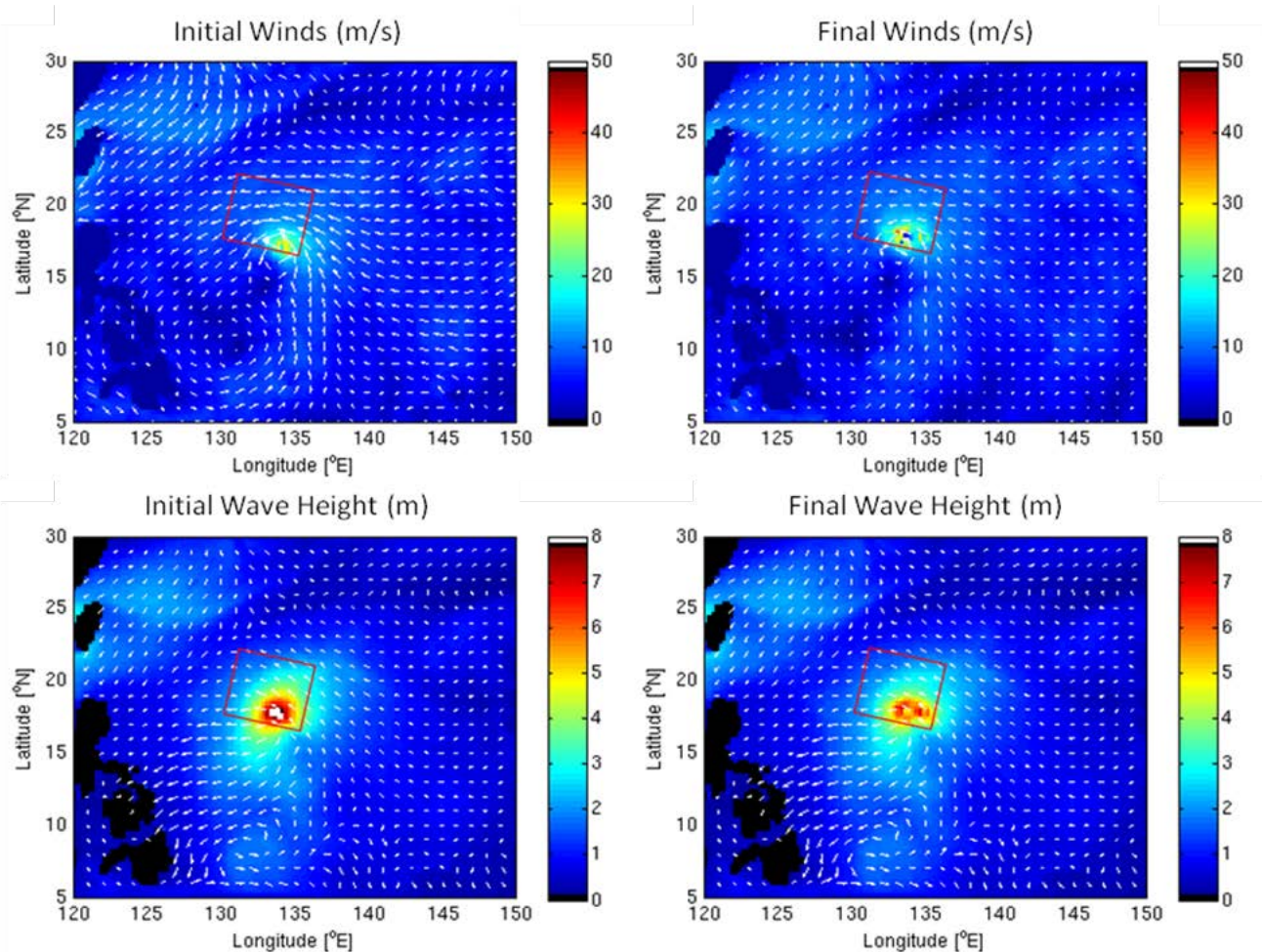


Figure 5. Comparison of first-guess and final estimated winds and wave heights for the time of the SAR image. The first-guess winds have a maximum of 32 m/s, while the final estimated winds have a maximum of 51 m/s, which compares favorably with the best-track estimate of 38-47 m/s. The final estimate of the significant wave height has decreased to about 7 m from 9 m for the first-guess winds; this is due to a reduction in estimated wind speed at earlier times.

Figure 5 shows a comparison of the initial-guess and final estimated winds and significant wave height for 2100 GMT on 15 October, the time of the SAR data collection. For the first-guess (ECMWF) winds, the maximum wind speed is about 32 m/s. For the final estimate, the maximum wind speed is 51 m/s. This result is in good agreement with the best-track estimate of 38-47 m/s for the maximum sustained surface winds. It should be noted that the structure of the storm has been modified in the final results with the high-wind region moving roughly one degree to the west. While the maximum winds have increased, areas of low wind speed have also been produced just behind the maximum wind region, as well as earlier in time. As a result of these decreased winds, there has been a decrease in the significant wave height from about 9 m for the initial-guess winds to roughly 7 m for the final estimate.

IMPACT/APPLICATIONS

If successful, the algorithm developed here will enable improved operational prediction of tropical cyclone evolution.

RELATED PROJECTS

This program is part of the ITOP Departmental Research Initiative

REFERENCES

- Booij, N., Ris, R.C. & Holthuijsen, L.H. 1999 A third-generation wave model for coastal regions: 1. Model description and validation. *J. Geophys. Res.* **104**, 7649.
- Donelan, M. A., B. K. Haus, N. Reul, W. J. Plant, M. Stiassnie, H. C. Graber, O. B. Brown & E. S. Saltzman, 2004: On the limiting aerodynamic roughness of the ocean in very strong winds. *Geophys. Res. Letters* **31**, L18306.
- Hasselmann, K. & Hasselmann, S. 1991 On the nonlinear mapping of an ocean-wave spectrum into a synthetic aperture radar image spectrum and its inversion. *J. Geophys. Res.* **96**, 10 713–10 729.
- Ris, R.C., L.H. Holthuijsen and N. Booij 1999 A third-generation wave model for coastal regions: 2. Verification. *J. Geophys. Res.* **104**, 7667.
- Walker, David T. 2006 *Assimilation of SAR imagery in a nearshore spectral wave model*. Report No. 200306-F. General Dynamics Advanced Information Systems, Ypsilanti, MI.
- Wu, J., 1982: Wind-stress coefficients over sea surface from breeze to hurricane, *J. Geophys. Res.* **87**, C12, 9704-9706.